Available online at www.sciencedirect.com
ScienceDirect
Trans. Nonferrous Met. Soc. China 35(2025) 1996−2007
Transactions of Nonferrous Metals Society of China
www.tnmsc.cn

Core−shell Bi@ mesoporous carbon nanospheres as high rate and long life anodes for sodium ion batteries

Wu YANG[1], Zhe-wei YANG[1], Chao-hui WANG[1], Hai-nan BIAN[1], Yue-de PAN[1], Gang LI[1], Kai-ying WANG[2], Jie-xi WANG[3,4]

1. Institute of Energy Innovation, College of Materials Science and Engineering, Taiyuan University of Technology, Taiyuan 030024, China;
2. Department of Microsystems, University of South-Eastern Norway, Horten 3184, Norway;
3. School of Metallurgy and Environment, Central South University, Changsha 410083, China;
4. National Engineering Research Centre of Advanced Energy Storage Materials, Changsha 410205, China

Received 5 February 2024; accepted 10 December 2024

Abstract: In order to restrain the huge volume expansion of bismuth (Bi) anodes in sodium ion batteries (SIBs), the core−shell structure Bi@mesoporous carbon nanospheres (Bi@mC) composite was designed and prepared by sol−gel method coupled heat treatment. Structural characterization displays that the average diameter of the as-prepared Bi@mC composites is about 200 nm and thickness of the N-doped mesoporous carbon shells is 20−30 nm. Electrochemical test and kinetic analysis results show that the mesoporous carbon shell can not only effectively relieve the stress caused by volume expansion of Bi and protect active material from pulverization caused by the stress during charging/discharging process, but also facilitate quick diffusion of sodium ions, thus improving rate and cycling performance. Bi@mC delivers a high specific capacity of 279 mA·h/g and a capacity retention of 97.6% after 3500 cycles at a current density of 5 A/g. Even at a high current density of 20 A/g, Bi@mC can still maintain a high specific capacity of 266 mA·h/g. Additionally, the Bi@mC//NVP full button sodium-ion batteries (SIBs) assembled using Bi@mC anode and $Na_3V_2(PO_4)_3$(NVP) cathode deliver an energy density of 182 W·h/kg.
Key words: sodium ion battery; bismuth; core−shell structure; sol−gel method; kinetic analysis

1 Introduction

Sodium-ion batteries (SIBs) have been drawing great attention as the most promising substitute for lithium-ion batteries (LIBs) for large-scale energy storage due to the natural abundance and low cost of sodium [1−3]. Although numerous anode materials have been investigated, their capacity, rate capability and cyclic performance could not meet the practical needs. It is urgent to explore the anode materials that could effectively facilitate quick insertion and extraction of sodium ions. Due to the appropriate operating voltage range and high specific capacity, the alloy-type anode materials (Sn [4,5], Sb [6,7], P [8,9], and Bi [10,11], etc.) have been investigated. Among them, Bi has great application potential with the advantages of high theoretical mass specific capacity (385 mA·h/g) and volume specific capacity (3800 mA·h/L) [12]. Meanwhile, Bi (d_{003}=3.95 Å) has a special layered crystal structure that makes it easier for the insertion and extraction of large-sized sodium ions. As a result, the volume expansion of Bi-based anode materials during charging/discharging is smaller than that of other alloy-type metal anode materials [13,14].

Corresponding author: Zhe-wei YANG, E-mail: yangzhewei@tyut.edu.cn; Gang LI, E-mail: ligang02@tyut.edu.cn
https://doi.org/10.1016/S1003-6326(25)66796-3

However, a relatively huge volume expansion could be generated during charging/discharging of Bi, which pulverizes the active material and detaches it from the collectors [15]. Constructing nanostructures and composites are the two most effective methods to boost the electrochemical performance of Bi-based anodes. YANG et al [16] prepared Bi@C nanocomposites by aerosol spray pyrolysis. However, a low capacity of 90 mA·h/g at 2 A/g and 123.5 mA·h/g after 100 cycles were observed for Bi@C nanocomposites. HWANG et al [17] designed a Bi-reduced graphene oxide composite (Bi/RGO), where Bi nanoparticles were attached to the surface of the RGO to mitigate the expansion of volume, and the Bi/RGO composite delivered a capacity of 200 mA·h/g at 50 mA/g. CHENG et al [18] designed the Bi@3DGF composite with Bi nanoparticles embedded into the three dimensional graphene framework (DGF), which exhibited excellent rate performance (194 mA·h/g at 20 A/g). Although much work on the structural design of the Bi-based anode has been done, the electrochemical stability is still not satisfactory. The suitable nanostructures need to be designed. The structure could not only mitigate the significant expansion of the Bi anode material during charging and discharging, but also facilitate the efficient movement of sodium ions.

Herein, the core−shell Bi@mesoporous carbon nanospheres (Bi@mC) were prepared by the simple sol−gel and heat treatment methods, using surfactant cetyltrimethylammonium bromide (CTAB) as a mesoporous template and polyvinylpyrrolidone (PVP) as a carbon source. The core−shell structure possesses several advantages as follows: (1) the mesoporous carbon shell can efficiently alleviate the stress resulting from volume expansion and avoid the disintegration of active material during charging or discharging; (2) the mesoporous carbon shell with open-ended structure could promote the rapid diffusion of sodium ions and ensure the active material is completely immersed in the electrolyte, which contributes to the excellent electrochemical performance. Furthermore, electrochemical impedance spectroscopy (EIS), cyclic voltammetry (CV) and the galvanostatic intermittent titration method (GITT) revealed its electrochemical kinetics process. The as-prepared Bi@mC was used as anode material to assemble a full button cell, and its electrochemical performance was also studied.

2 Experimental

2.1 Preparation of Bi nanospheres

Bi nanospheres were synthesized by the solvothermal method. 0.75 mmol of $Bi(NO_3)_3·5H_2O$ and 0.06 mmol of poly(vinylpyrrolidone) (relative molecular mass of 10000) were added to a mixture of 50 mL of ethylene glycol and 10 mL of nitric acid (1 mol/L), and stirred for 0.5 h. Then, they were transferred to a 100 mL reactor and kept at 150 °C for 12 h. Bi nanoparticles were obtained after washing, centrifugation and vacuum drying.

2.2 Preparation of Bi@mSiO$_2$

150 mg of Bi nanosphere and 225 mg of CTAB were dispersed in ethanol and deionized water, and stirred for 0.5 h. The pH was adjusted to alkalinity by adding appropriate amount of ammonia. Then, 120 uL of ethyl orthosilicate (TEOS) was added and stirred for 6 h at room temperature. At last, the Bi@mSiO$_2$ was obtained after removing the CTAB by condensation and reflux in anhydrous ethanol solution at 70 °C.

2.3 Preparation of Bi@mC

The above Bi@mSiO$_2$ was dissolved in PVP solution by ultrasonic and the mass ratio of PVP to Bi@mSiO$_2$ was 1.5. Then, the Bi@mSiO$_2$@C precursor was prepared by freeze-drying. After calcination treatment in 5% Ar/H_2 atmosphere at 800 °C for 3 h and following removal of SiO_2 by NaOH solution, the Bi@mC was obtained finally.

2.4 Material characterization

An X-ray diffractometer (Malvem Panalytical B.V Empyrean) was used to examine XRD patterns in the 2θ range of 10°−90° at a scan rate of 10 (°)/min. A thermo Scientific's ESCALAB Xi^+ instrument was applied to the X-ray photoelectron spectroscopy (XPS) testing. A Renishaw invia reflex spectrometer was used to record the Raman scattering spectra. The microphysical morphology of the samples was characterized by SEM (Gemini SEM 300) and TEM (JEOL, JEM−2100 F). TG analysis was performed using an STA−449−F5 simultaneous thermal analyzer. The APSP 2460 multi-station extended specific surface area and porosity analyzer was used to analyze the materials' nitrogen adsorption and desorption isotherms, as

well as to calculate the specific surface area and pore size distribution.

2.5 Electrochemical tests

The electrode slurry was made by combining a 7:2:1 mass ratio of Bi@mC composite with a polyvinylidene fluoride (PVDF) binder and Super P in N-methylpyrrolidone (NMP). Then, electrode was prepared by coating the slurry onto copper foils and dried at 120 °C for 12 h in a vacuum drying oven. The loading mass of active material was ~1.2 mg/cm^2. The $Na_3V_2(PO_4)_3$ (NVP) cathode electrode was prepared by the same method; however, the current collector was aluminum foil. The loading of NVP active material was 2.5−3 mg/cm^2. The electrochemical performance was tested in CR2032 coin cells. For half-cells, metallic sodium sheets were used as counter electrodes and reference electrode. The electrolyte was made of 1 mol/L $NaPF_6$ dissolved in ethylene glycol dimethyl ether (DME). Glass fiber (Whatman GF/D) was used as separator. For full-cells, NVP was selected as cathode and the Bi@mC was used as anode. The cathode-to-anode mass ratio was designed to be 2.5. The cyclic voltammetry (CV) test was conducted using a CHI660 electrochemical workstation. An Neware battery test was conducted to accomplish the galvanostatic charging/discharging (GCD) test.

3 Results and discussion

3.1 Structural characteristics

Figure 1 depicts the procedure for synthesizing Bi@mC. Initially, the Bi nanospheres (Bi NSs) were synthesized using a simple solvothermal method. Subsequently, the Bi NSs were enveloped with a consistent layer of mesoporous silica, which was synthesized by the sol−gel method, using the surfactant CTAB as the mesoporous template and TEOS as the SiO_2 precursor. Whereafter, the obtained material was impregnated in PVP solution, which could penetrate into the mesopores of the silica layer and served as the carbon source. Finally, the core−shell Bi@mC composites were obtained by carbonizing at 800 °C in the Ar/H_2 atmosphere, followed by NaOH treatment.

Figures 2(a) and (b) show the SEM images of the pristine Bi nanospheres and Bi@mC composites, respectively. Compared with the pristine Bi nanospheres, the Bi@mC composites clearly possess a thin layer of coating on their surface and the average diameters of them are also significantly different. The average diameter of the Bi@mC composites is about 200 nm, which is larger than that of the pristine Bi nanoparticles (150 nm). TEM images (Figs. 2(c−e)) and Fig. S1 in Supplementary Information show that the core Bi nanoparticles are encapsulated in the carbon shell within the range of 20−30 nm. The lattice spacing is about 0.32 nm, which corresponds to the (012) crystalline surface of the Bi nanoparticles, and the carbon shell shows the disordered porous structure. Meanwhile, the high-angle annular dark field (HADDF) images and the energy dispersive X-ray spectroscopy (EDS) elemental mappings of Bi@mC composites are shown in Figs. 2(f−j), which demonstrate that the Bi nanospheres are encapsulated in the N-doped porous carbon shells.

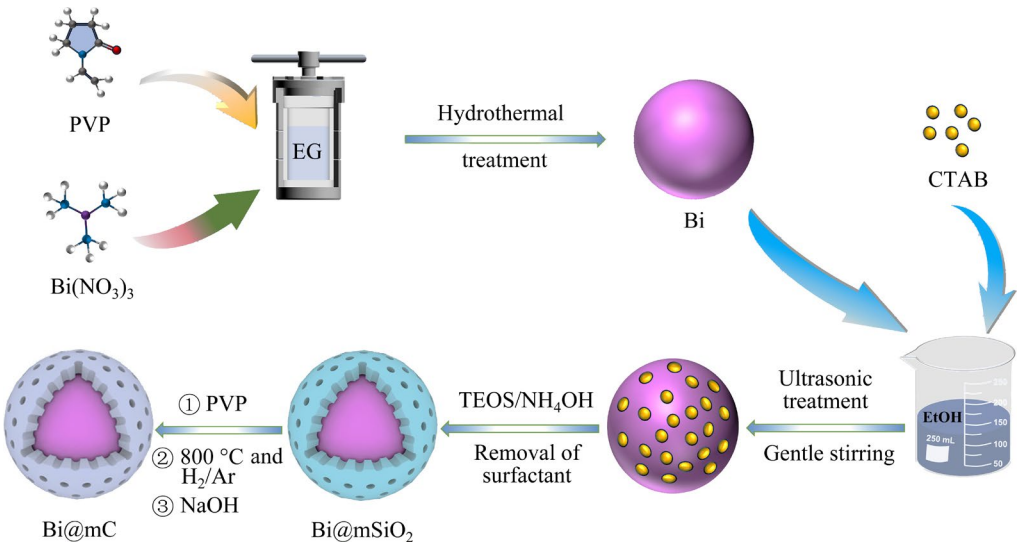

Fig. 1 Schematic illustration of preparation process for Bi@mC

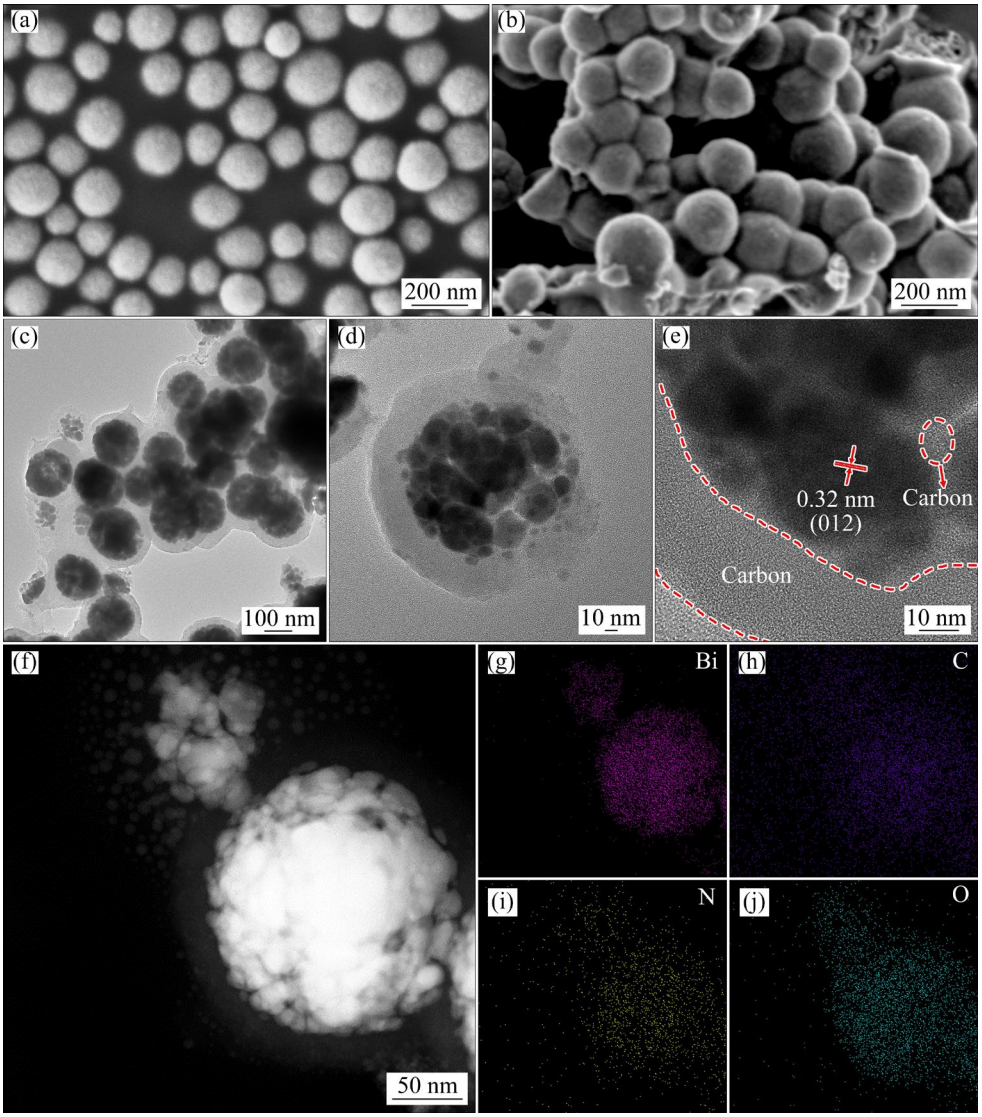

Fig. 2 (a, b) SEM images of Bi and Bi@mC, respectively; (c−e) TEM images of Bi@mC; (f–j) HADDF-STEM image and corresponding elemental mappings of Bi@mC

The structure of Bi@mC was analyzed by X-ray diffraction (XRD) and Raman spectra. The high crystalline Bi phase (JCPDS No. 85-1329) is clearly confirmed by the XRD pattern of the Bi@mC, as shown in Fig. 3(a). According to the Raman spectra (Fig. 3(b)), Bi@mC shows the characteristic peaks at ~1350 and ~1590 cm^{-1} corresponding to the sp^3 configuration (D band) and the sp^2 graphitic configuration (G band) [19], respectively. Intensity ratio between G and D bands (I_G/I_D) of 1.05 suggests that the partially graphitized N-doped carbon layer may improve the conductivity [20]. According to the thermo-gravimetric (TG) analysis (Fig. 3(c)), the Bi content in the Bi@mC composite is 72.7 wt.%.

X-ray photoelectron spectroscopy (XPS) is employed to further investigate the chemical composition of Bi@mC. Wide scan XPS spectrum (Fig. 4(a)) indicates that the Bi@mC composite contains C, N, O and Bi. The high-resolution C 1s XPS spectrum of Bi@mC (Fig. 4(b)) is analyzed and divided into three distinct components: C—O at 288.1 eV, C—N at 285.7 eV and C—C at 284.8 eV, respectively. High-resolution N 1s XPS spectrum of Bi@mC (Fig. 4(c)) is also fitted into three major peaks corresponding to quaternary N (400.0 eV, N-Q), pyrrolic N (399.6 eV, N-5) and pyridinic N (397.0 eV, N-6), respectively [21,22]. N is mainly derived from the PVP, which forms N-doped carbon shell when carbonized at high temperatures. N-doping could increase sodium ions storage sites and accelerate the kinetics [23]. Additionally, the

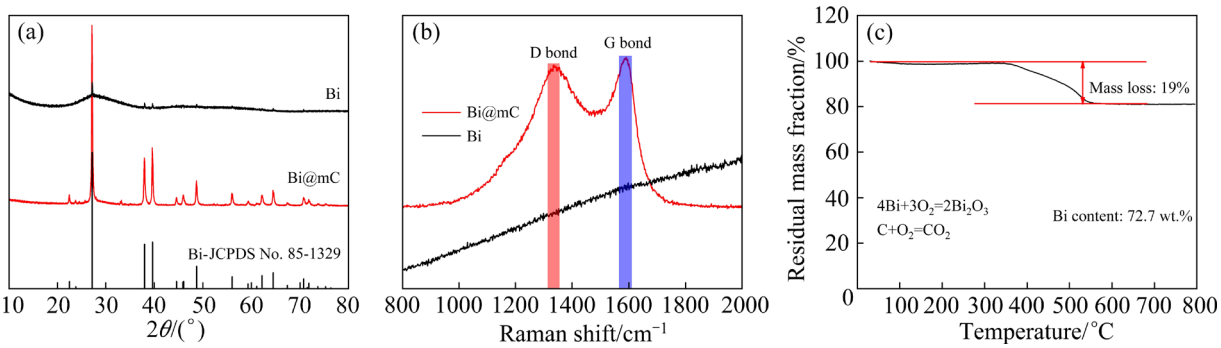

Fig. 3 (a) XRD patterns of Bi and Bi@mC; (b) Raman spectra of Bi and Bi@mC; (c) TG curve of Bi@mC

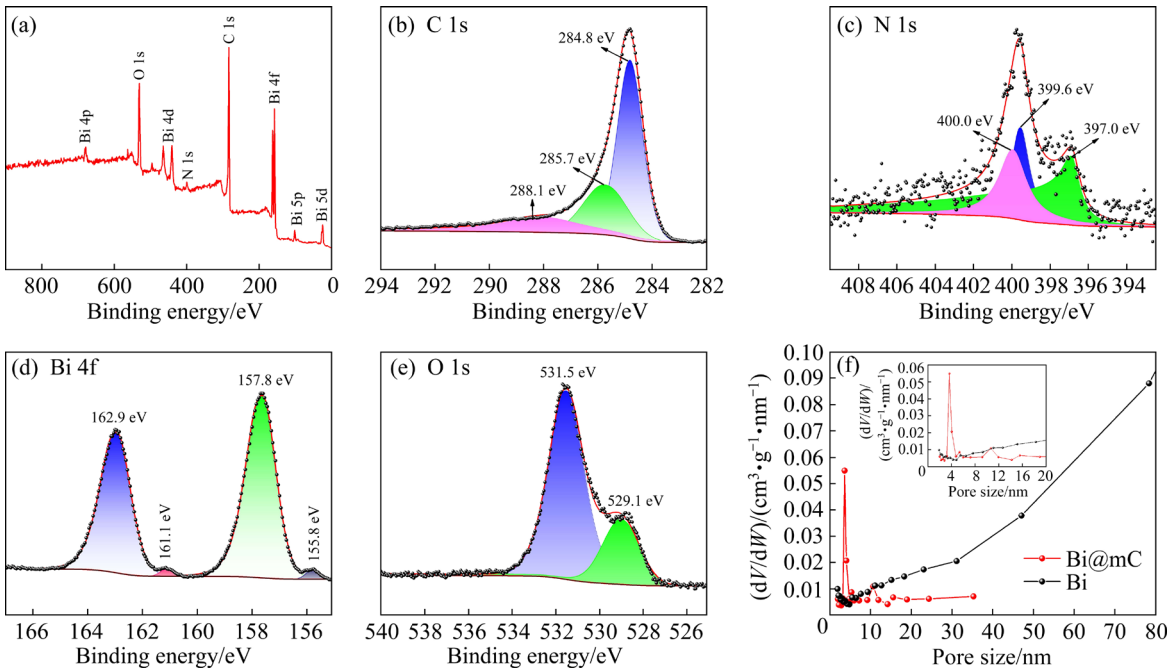

Fig. 4 (a) Wide scan XPS spectrum of Bi@mC; (b−e) High-resolution XPS spectra of Bi@mC; (f) Pore size distribution determined by BJH model of Bi@mC and Bi

Bi—O bonds at 162.9 and 157.8 eV in the Bi 4f spectrum (Fig. 4(d)), the C—O bonds at 288.1 eV in the C 1s spectrum and the Bi—O—C bond at 529.1 eV in the O 1s spectrum (Fig. 4(e)) could be observed, indicating the existence of Bi oxides in Bi@mC composites. According to the previous work [24,25], The surface of Bi nanoparticles is inevitably oxidized to Bi_2O_3 during the exposure of Bi@mC to air. According to the testing mechanism of XPS, the oxidation of Bi occurs only on the surface of Bi and the content of Bi_2O_3 is very low. Trace Bi_2O_3 exists in the Bi@mC composite due to the unavoidable oxidization, which has little effect on its electrochemical properties.

The isotherms for nitrogen adsorption and desorption are shown in Fig. S2 in Supplementary Information, while the pore size distribution (PSD) obtained using the BJH model is shown in Fig. 4(f). Observations of type IV isotherms according to the Brunner classification, suggest the presence of mesopores for Bi@mC. The specific surface area (SSA) of Bi@mC is 7.471 m^2/g, and its mesopore volume is 0.013 cm^3/g. These values are lower than those of Bi metal, which has an SSA of 11.082 m^2/g and a mesopore volume of 0.054 cm^3/g. The average pore size of Bi@mC is concentrated at ~4 nm, nevertheless, the macropore (>50 nm) is dominant for Bi metal.

3.2 Electrochemical performance of Bi@mC

The electrochemical performance of Bi@mC was studied using the half-cells with a sodium metal

counter electrode and reference electrode. Figure 5(a) shows the GCD curves of Bi@mC during the initial three cycles at 0.05 A/g. The Bi@mC delivers an initial charge capacity of 361 mA·h/g with an initial coulombic efficiency (ICE) of 53.9%. The initial loss in capacity may be due to the formation of a solid electrolyte interphase (SEI) layer and the occurrence of side reactions between the active materials and the electrolyte. Figure S3 in Supplementary Information shows the initial charge and discharge curves of Bi@mC and Bi. The ICE of Bi@mC (53.9%) is higher than that for the pure Bi (47.4%), which could be attributed to the fact that the mesoporous carbon coating helps to construct a stable SEI membrane and prevent the occurrence of large side reactions between the electrode and electrolyte. Additionally, two obvious flats at ~0.66 and ~0.47 V during the second discharge process, respectively are associated with the interaction between sodium ions and bismuth, which could be demonstrated by the CV curves of Bi@mC (Fig. 5(b)). After the first cycle, two distinct sets of well-defined redox peaks were found at 0.77 V/0.66 V and 0.60 V/0.47 V, which correspond to the Bi⇌NaBi and NaBi⇌Na_3Bi reactions, respectively [26].

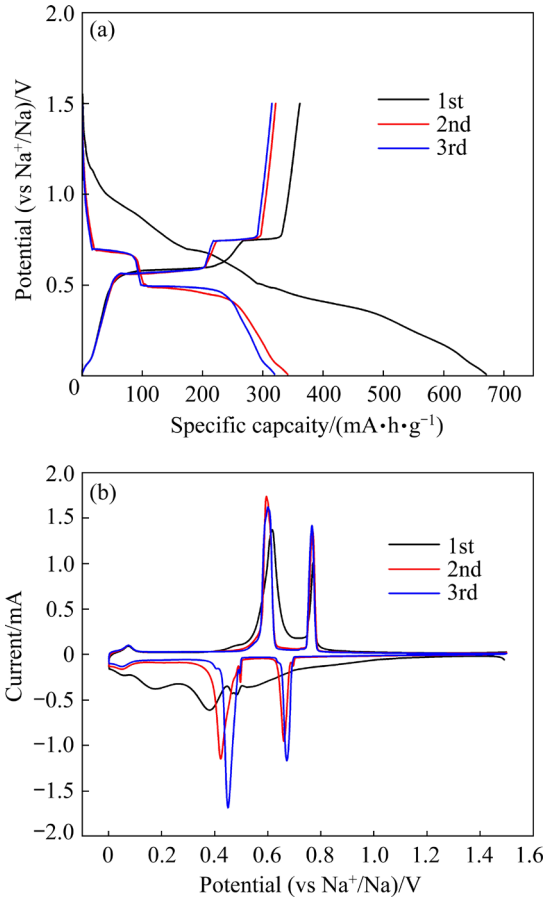

Fig. 5 (a) GCD curves of Bi@mC during initial three cycles at 0.05 A/g; (b) CV curves of Bi@mC during initial three cycles at 0.1 mV/s

Figure 6(a) presents the rate capability of Bi@mC and Bi at different current densities. At 0.05 A/g, Bi@mC displays a reversible capacity of 306 mA·h/g. It is exciting that there is little capacity decay for Bi@mC with the increase of current density. Bi@mC delivers a reversible capacity of 285, 281, 283, 286, 287, 284 and 277 mA·h/g at 0.1, 0.2, 0.5, 1, 2, 5, and 10 A/g, respectively. Even at a high current density of 20 A/g, the reversible capacity could reach 266 mA·h/g and the discharging time is only 48 s. Additionally, as shown in the GCD curves at different current densities (Fig. 6(b)), Bi@mC still displays the double-platform feature of the Bi-based material even at high current density of 20 A/g, indicating a fast kinetic process. For comparison, the pure Bi metal electrodes show the poor rate capability, which delivers a reversible capacity of 245, 171, 103, 81, 68, 56, 40, 27 and 11 mA·h/g at 0.05, 0.1, 0.2, 0.5, 1, 2, 5, 10 and 20 A/g (Fig. 6(a) and Fig. S4 in Supplementary Information). To our knowledge, the rate performance of Bi@mC is also much better than that of some Bi-based materials reported in literatures, such as Bi@C [16], Bi@graphene [27], Bi@3DGF [18], 2D FLB [28], Bi/Ni [29], Bi/C nanofibers [30], and Bi@ N−C [20] (Fig. 6(c)) (Table S1 in Supplementary Information).

Figures 6(d) and (e) indicate the cycling performance and coulombic efficiency of the Bi@mC composite at 1 and 5 A/g, respectively. The decline in capacity during the first 20 cycles may be attributed to the instability at the interface during the activation phase. After 20 cycles, the capacity tends to stabilize and the coulombic efficiency could keep at ~100% in the subsequent cycles. After 350 cycles at 1 A/g, Bi@mC could deliver a high capacity of 303 mA·h/g, which is much higher than that of Bi metal (Fig. S5 in Supplementary Information). Impressively, Bi@mC has a notable specific capacity of 279 mA·h/g and maintains a capacity retention of 97.6% even after undergoing 3500 cycles at 5 A/g. Additionally, as shown in the GCD curves for different cycles (Figs. S6 and S7 in Supplementary Information), the profile featured the double-platform did not change significantly after

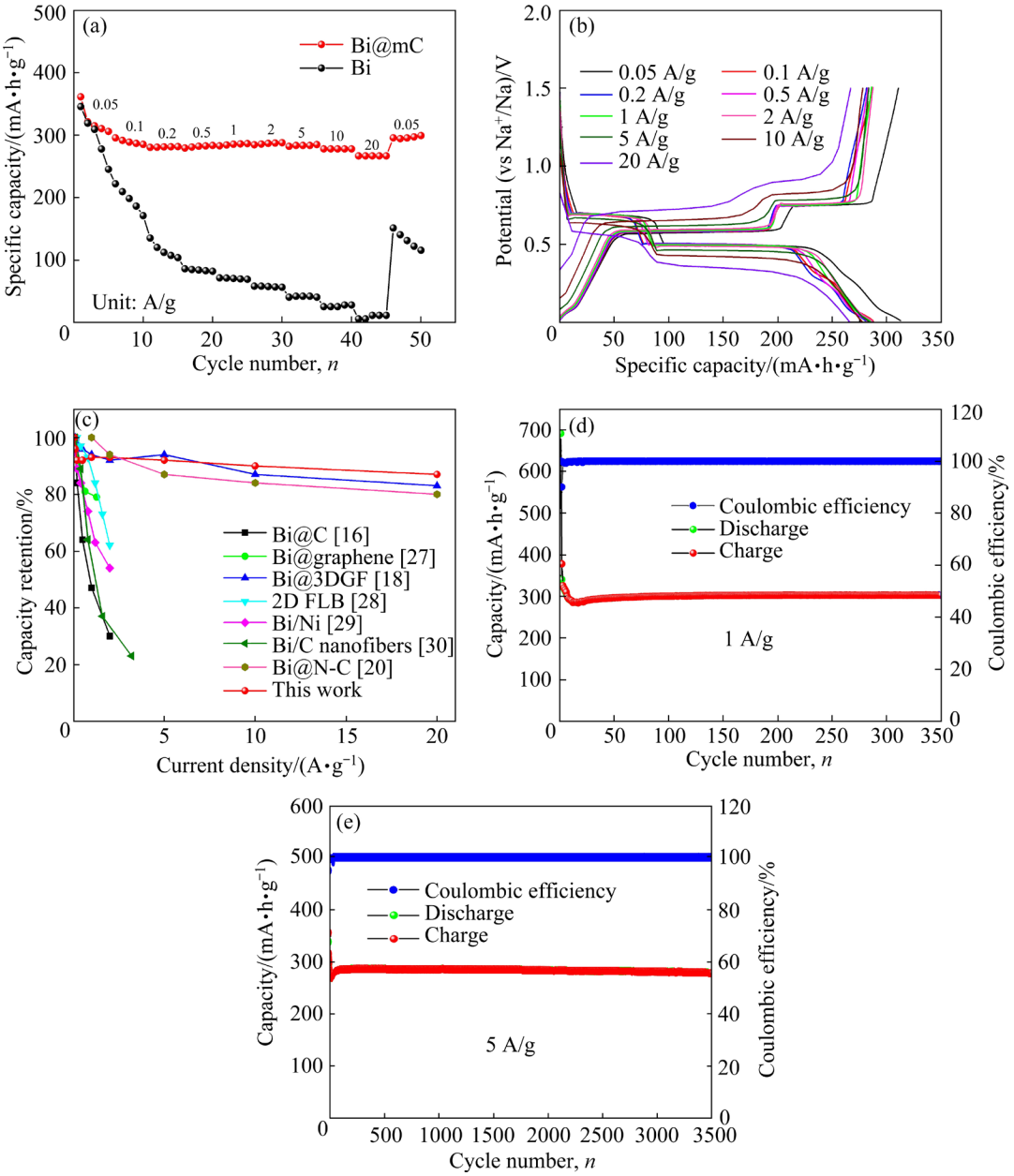

Fig. 6 (a) Rate performance of Bi@mC and Bi; (b) GCD curves of Bi@mC at different current densities; (c) Comparison of rate capability with reported anode materials for SIBs; (d, e) Cycling stability and coulombic efficiency of Bi@mC at 1 and 5 A/g, respectively

different cycles at 1 and 5 A/g, indicating its outstanding cycling stability.

Ultimately, Bi@mC has exceptional rate capability and cycle performance primarily due to its core−shell structure. The mesoporous carbon shell serves multiple functions: it alleviates stress resulting from volume expansion and prevents the active material from being pulverized during charging and discharging. Additionally, it facilitates the rapid diffusion of sodium ions from the electrolyte, thereby enhancing the rate and cycling performance of the system.

3.3 Electrode kinetic analysis results

In order to delve further into the electrochemical kinetics process, a series of experiments were conducted, including EIS, CV tests at various scan rates and the GITT. Figure 7(a) displays the Nyquist plots after 5 cycles at 0.05 A/g for Bi@mC and Bi. Compared to pure Bi metal, Bi@mC exhibits a lower charge-transfer resistance (R_{ct}) of 3.36 Ω, indicating its faster kinetic process of Bi@mC. Figure 7(b) displays the CV curves at the scan rates of 0.3−0.7 mV/s for Bi@mC. The characteristic redox peaks could still be preserved

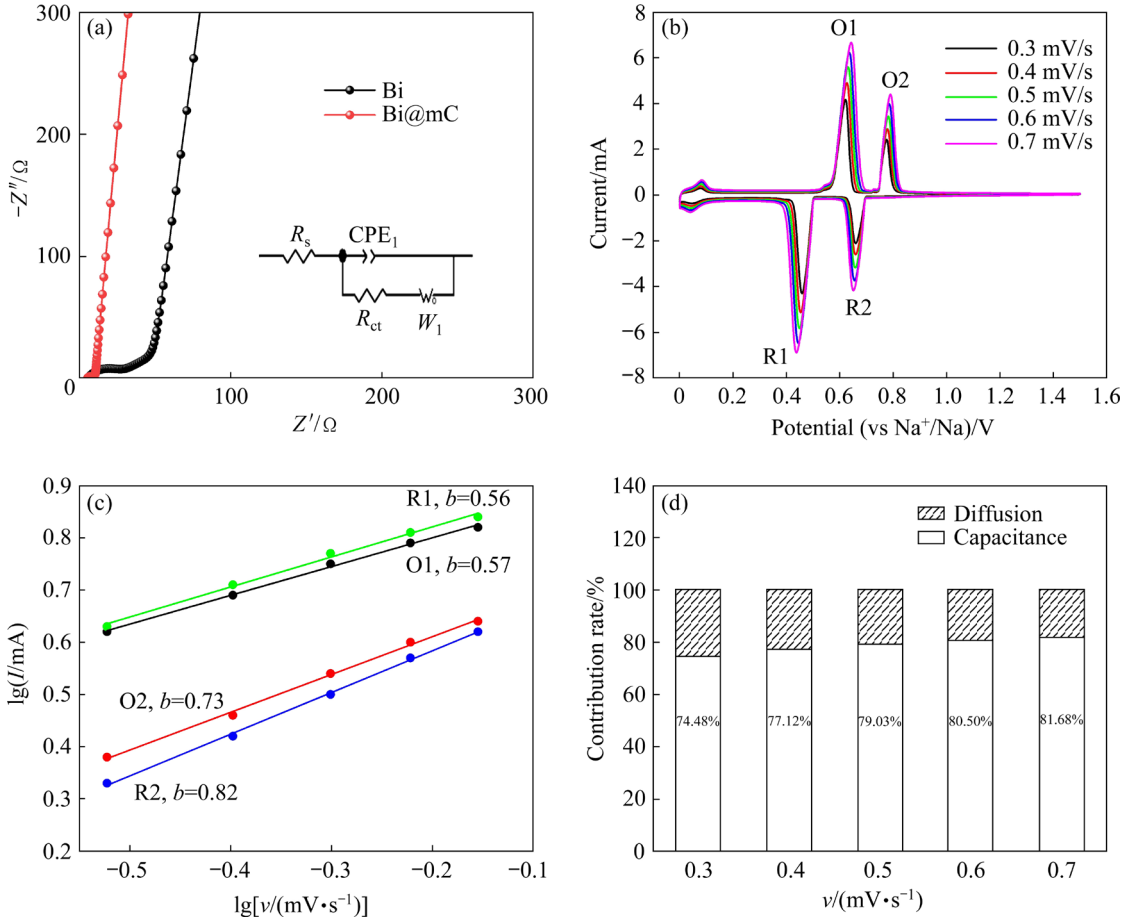

Fig. 7 (a) Nyquist plots of Bi and Bi@mC after 5 cycles at 0.05 A/g; (b) CV curves at various scan rates; (c) Relationship between peak current (I) and scan rate (v) in logarithmic format; (d) Diffusion and capacitance contribution rates of Bi@mC at different scan rates

well, suggesting small polarization and fast kinetics. In general, the scan rate determines the current response, as shown by the following equations [31,32]:

$$I=av^b \tag{1}$$

$$\lg I=b\lg v+\lg a \tag{2}$$

where a and b are constants that may be adjusted, I is the current response, and v is the scan rate. If b=1, the surface-induced capacitance process limits the electrode response, whereas when b=0.5, the diffusion-controlled process controls it.

Figure 7(c) demonstrates the $\lg I$–$\lg v$ plots of redox peaks (O1/R1, O2/R2) for Bi@mC. The b values corresponding to the four redox peaks, O1, O2, R1, and R2, are 0.57, 0.73, 0.56, and 0.82, respectively, which indicate that the electrode process of Bi@mC is controlled by the pseudo-capacitance and the diffusion process together. In addition, the capacitance contribution is further quantitatively separated from the capacity using the following equation [33]:

$$I(v)=k_1v+k_2v^{1/2} \tag{3}$$

where both k_1 and k_2 are constants, and the values of k_1v and $k_2v^{1/2}$ represent the contributions of the capacitance and diffusion, respectively. Figure 7(d) shows the capacitance contribution at different scan rates from 0.3 to 0.7 mV/s. The capacitance contribution rises as the scan rate increases. At a scan rate of 0.7 mV/s, the capacitance contribution reaches up to 81.68%, which supports the explanation for its exceptional rate capacity.

Figure 8(a) shows the GITT curves for Bi@mC and Bi electrodes. After cycling 5 times, the GITT test was performed at 0.05 A/g for 30 min of constant current charging/discharging, followed by 5 h of shelving to return the anode material to a thermodynamically stable state. The Bi@mC composite electrode has a lower overpotential

compared to the pure Bi metal electrode, indicating a fast kinetic process for Bi@mC. Figure 8(b) illustrates the diffusion coefficients (D) of sodium ions in both Bi@mC composite and Bi metal electrodes, which are calculated by GITT curves using the following equation [34]:

$$D=\frac{4}{\pi\tau}\left(\frac{m_b V_M}{M_B S}\right)^2\left(\frac{\Delta E_s}{\Delta E_t}\right)^2 \left(\tau \ll \frac{L^2}{D}\right) \quad (4)$$

where τ is the current pulse time, m_b, M_B, and V_M are the mass, molar mass, and molar volume of the active ingredient, respectively, S is the electrode area, ΔE_s represents the voltage change caused by the pulse, ΔE_t represents the voltage change of the constant current charging/discharging, and L is the sodium ion diffusion length. The variation trend of the diffusion coefficients at different potentials for Bi@mC is similar to that for Bi metal. However, Bi@mC shows higher diffusion coefficients than Bi metal, suggesting its fast kinetic process, because the mesoporous carbon shell could provide convenient channels for Na ion diffusion.

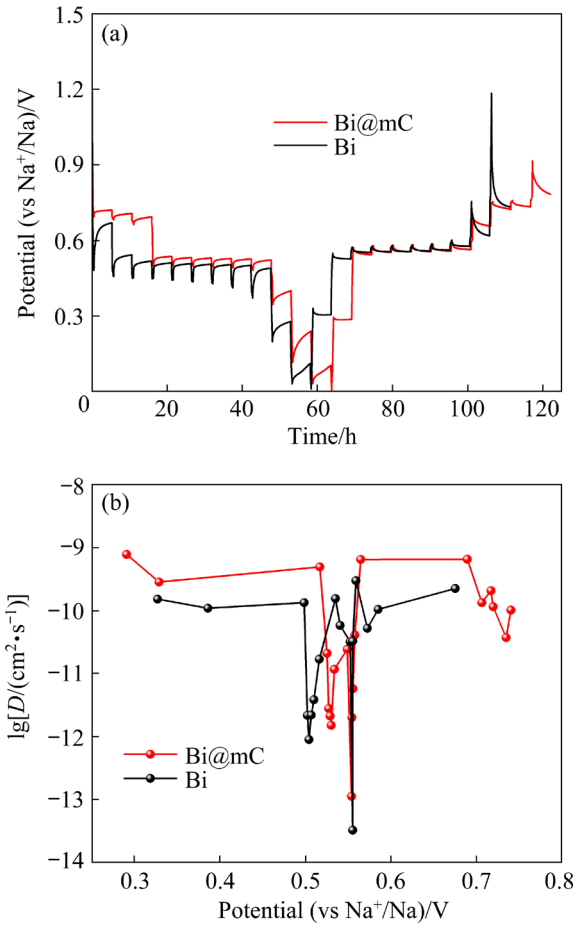

Fig. 8 (a) GITT curves for Bi@mC and Bi; (b) Diffusion coefficients of Bi@mC and Bi calculated from GITT curves

3.4 Electrochemical performance of full cell

Given the outstanding electrochemical performance of the Bi@mC electrode in half cells, we were motivated to assess its potential applicability in a full cell. The full SIB assembled by a Bi@mC as anode and a $Na_3V_2(PO_4)_3$ (NVP) as cathode is shown in Fig. 9(a). The NVP exhibits a voltage plateau at around 3.4 V and maintains a steady discharge/charge capacity of roughly 110 mA·h/g for 100 cycles at 0.1 A/g (Fig. S8 in Supplementary Information). Figure 9(b) displays the GCD curves of both the half cells and the full cell. During the charging process, the Na ions de-intercalated from NVP cathode are intercalated into the porous Bi@mC anode in full cell. Consequently, the de-insertion of Na ions from Na_xBi and the insertion of Na ions to NVP happen during the discharge process. Bi@mC//NVP delivers a reversible capacity of 67.8, 62.7, 54.4, 48.2, 43.7 and 37.4 mA·h/g at 0.05, 0.1, 0.2, 0.5, 1 and 2 A/g, respectively (Fig. 9(c)). The Bi@mC// NVP full SIBs deliver an energy density of 182 W·h/kg based on the total mass of anode and cathode materials. After 100 cycles at 0.5 A/g, the cycle retention is 77.5% (Fig. 9(d)). Additionally, the button full-cell could drive a small electric fan, indicating its practical potential in SIBs.

4 Conclusions

(1) The core−shell Bi@mesoporous carbon nanospheres (Bi@mC) composites are successfully prepared by the simple sol−gel and heat treatment methods. The Bi nanospheres are encapsulated in the N-doped mesoporous carbon shells. The average diameter of the Bi@mC composites is about 200 nm and thickness of the N-doped mesoporous carbon shells is 20−30 nm. Bi@mC shows the mesoporous structures and the average pore is concentrated at ~4 nm.

(2) The N-doped mesoporous carbon shells facilitate Na ion transport, enhancing kinetic performance, while simultaneously mitigating volume expansion of Bi, thus improving cycle stability. Bi@mC shows a high specific capacity of 266 mA·h/g when subjected to a high current density of 20 A/g. Bi@mC demonstrates a capacity

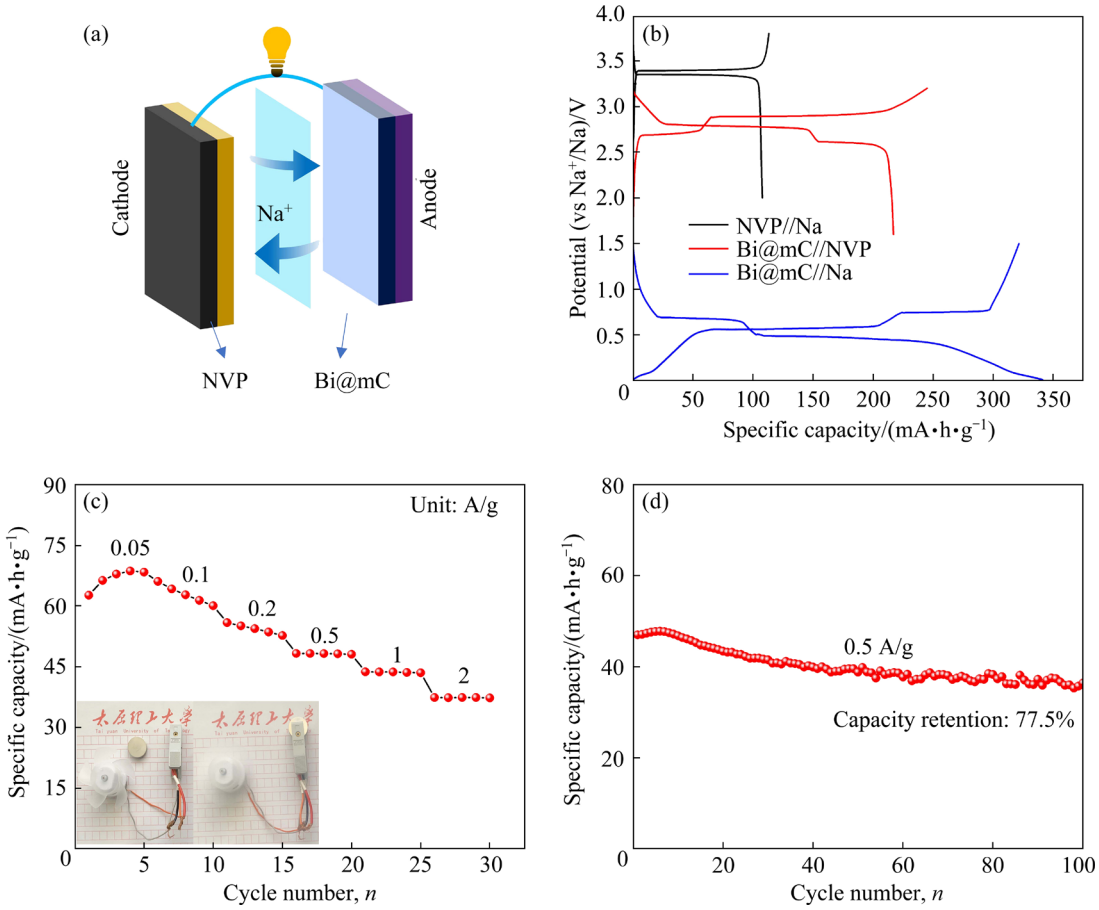

Fig. 9 (a) Schematic illustration of full cell with NVP as cathode and Bi@mC as anode; (b) GCD profiles of half cell and full cell; (c) Rate capability of full cell; (d) Cycling performance of full cell

retention of 97.6% after undergoing 3500 cycles at 5 A/g.

(3) The Bi@mC//NVP full SIBs using a Bi@mC anode and a $Na_3V_2(PO_4)_3$ cathode are assembled, which deliver an energy density of 182 W·h/kg.

CRediT authorship contribution statement

Wu YANG: Conceptualization, Methodology, Software, Investigation, Formal Analysis, Writing − Original draft; **Zhe-wei YANG:** Conceptualization, Funding acquisition, Resources, Supervision, Writing − Review & editing; **Chao-hui WANG:** Data curation; **Hai-nan BIAN:** Visualization, Investigation; **Yue-de PAN** and **Gang LI:** Resources, Supervision; **Kai-ying WANG:** Resources, Supervision, Writing − Review & editing; **Jie-xi WANG:** Visualization, Writing − Review & editing.

Declaration of competing interest

The authors declare that they have no known competing financial interests or personal relationships that could have appeared to influence the work reported in this paper.

Acknowledgments

The authors appreciate the support from National Natural Science Foundation of China (No. 52004179), the Fundamental Research Program of Shanxi Province, China (Nos. 202403021211028, 202303021211036), Shanxi Water and Wood New Carbon Materials Technology Co., Ltd., China, and Guangdong One Nano Technology Co., Ltd., China.

Supplementary Information

Supplementary Information in this paper can be found at: http://tnmsc.csu.edu.cn/download/18-p1996-2024-0239-Supplementary_Information.pdf.

References

[1] QIN Mu-lan, YIN Chang-yu, XU Wen, LIU Yang, WEN Jun-hao, SHEN Bin, WANG Wei-gang, LIU Wan-min. Facile synthesis of high capacity P_2-type $Na_{2/3}Fe_{1/2}Mn_{1/2}O_2$ cathode

material for sodium-ion batteries [J]. Transactions of Nonferrous Metals Society of China, 2021, 31(7): 2074−2080.

[2] QIN Mu-lan, LIU Wan-min, XIANG Yuan-jin, WANG Wei-gang, SHEN Bin. Synthesis and electrochemical performance of V_2O_5/NaV_6O_{15} nanocomposites as cathode materials for sodium-ion batteries [J]. Transactions of Nonferrous Metals Society of China, 2020, 30(8): 2200−2206.

[3] KUMAR P A, BHATNAGAR A. A review on anode materials for lithium/sodium-ion batteries [J]. Journal of Energy Chemistry, 2023, 83: 509−540.

[4] WU Xin, LAN Xue-xia, HU Ren-zong, YAO Yu, YU Yan, ZHU Min. Tin-based anode materials for stable sodium storage: Progress and perspective [J]. Advanced Materials, 2022, 34(7): e2106895.

[5] LI Bo, ZHANG Ting, WEI Shang-hai, GAO Wei. Nitrogen-doped carbon hollow spheres packed with multiple nano Sn particles for enhanced lithium storage [J]. Chemical Engineering Journal, 2022, 446: 136768.

[6] LIU Yi-hui, LIU Fu-sheng, LIU Bing-bing, XIAO Yao-yao, QIN Guo-hui, MA Jian-min. Dynamic hydrogen-bond network as a modulator of bismuth−antimony complex anodes for self-healable and wider temperature adaptive potassium ion batteries [J]. Angewandte Chemie International Edition, 2023, 62(19): e202300599.

[7] WANG Qi, LAI Yan-qing, LIU Fang-yang, JIANG Liang-xing, JIA Ming, WANG Xi-lun. Sb_2S_3 nanorods/porous-carbon composite from natural stibnite ore as high-performance anode for lithium-ion batteries [J]. Transactions of Nonferrous Metals Society of China, 2021, 31(7): 2051−2061.

[8] GE Jun-min, MA Cun-shuang, WAN Yan-hua, TANG Guo-chuan, DAI Hong-liu, SUN Shu-hui, CHEN Wei-hua. Electrocatalysis of Fe−N−C bonds driving reliable interphase and fast kinetics for phosphorus anode in sodium-ion batteries [J]. Advanced Functional Materials, 2023, 33(47): 2305803.

[9] CHENG Zhi-kang, TU Bing-tian, WU Ye, HUANG Hai-jun. High-pressure and high-temperature synthesis of black phosphorus-graphite anode material for lithium-ion batteries [J]. Electrochimica Acta, 2024, 473: 143510.

[10] LIU Miao, XING Yu-qi, WANG Jian-wen, WANG Dong, HUANG Lu, WU Xiao-man, LIU Zhi-xiao, WU Ying-peng. Besides the capacitive and diffusion control: inner-surface controlled bismuth based electrode facilitating potassium-ion energy storage [J]. Advanced Functional Materials, 2021, 31(27): 2101868.

[11] LIANG Ya-zhan, SONG Ning, ZHANG Zheng-chun-yu, CHEN Wei-hua, FENG Jin-kui, XI Bao-juan, XIONG Sheng-lin. Integrating Bi@C nanospheres in porous hard carbon frameworks for ultrafast sodium storage [J]. Advanced Materials, 2022, 34(28): 2202673.

[12] ZHANG Xiao-shan, QIU Xue-qing, LIN Jin-xin, LIN Ze-hua, SUN Shi-rong, YIN Jian, ALSHAREEF H N, ZHANG Wen-li. Structure and interface engineering of ultrahigh-rate 3D bismuth anodes for sodium-ion batteries [J]. Small, 2023, 19(35): e2302071.

[13] ZHANG Shao-jie, ZHANG Yi-ming, ZHANG Zi-yi, WANG Hui-li, CAO Yu, ZHANG Bao-shan, LIU Xin-yi, MAO Chong, HAN Xin-peng, GONG Hao-chen, YANG Zhan-xu, SUN Jie. Bi works as a Li reservoir for promoting the fast-charging performance of phosphorus anode for Li-ion batteries [J]. Advanced Energy Materials, 2022, 12(19): 2103888.

[14] SHEN Chao, CHENG Tian-le, LIU Chun-yan, HUANG Lu, CAO Meng-yang, SONG Gan-qiang, WANG Dong, LU Bin-gan, WANG Jian-wen, QIN Chi-chu, HUANG Xing-kang, PENG Ping, LI Xi-long, WU Ying-peng. Bismuthene from sonoelectrochemistry as a superior anode for potassium-ion batteries [J]. Journal of Materials Chemistry A, 2020, 8(1): 453−460.

[15] CHENG Xiao-long, SUN Ying-jie, LI Dong-jun, YANG Hai, CHEN Fei, HUANG Fan-yang, JIANG Yu, WU Ying, AN Xing-tao, YU Yan. From 0D to 3D: Dimensional control of bismuth for potassium storage with superb kinetics and cycling stability [J]. Advanced Energy Materials, 2021, 11(40): 2102263.

[16] YANG Fu-hua, YU Fan, ZHANG Zhi-an, ZHANG Kai, LAI Yan-qing, LI Jie. Bismuth nanoparticles embedded in carbon spheres as anode materials for sodium/lithium-ion batteries [J]. Chemistry, 2016, 22(7): 2333−2338.

[17] HWANG J, PARK J H, YOON C K, KIM J. One-pot synthesis of Bi-reduced graphene oxide composite using supercritical acetone as anode for Na-ion batteries [J]. Chemical Engineering Journal, 2020, 387: 124111.

[18] CHENG Xiao-long, LI Dong-jun, WU Ying, XU Rui, YU Yan. Bismuth nanospheres embedded in three-dimensional (3D) porous graphene frameworks as high performance anodes for sodium-and potassium-ion batteries [J]. Journal of Materials Chemistry A, 2019, 7(9): 4913−4921.

[19] WEI Shi-wei, LI Wei, MA Zi-zai, DENG Xiao-yang, LI Yong-feng, WANG Xiao-guang. Novel bismuth nanoflowers encapsulated in N-doped carbon frameworks as superb composite anodes for high-performance sodium-ion batteries [J]. Small, 2023, 19(46): 2304265.

[20] YANG Hai, XU Rui, YAO Yu, YE Shu-fen, ZHOU Xue-feng, YU Yan. Multicore-shell Bi@N-doped carbon nanospheres for high power density and long cycle life sodium- and potassium-ion anodes [J]. Advanced Functional Materials, 2019, 29(13): 1809195.

[21] LIU Xi, YU Xin-zhi, TONG Yong, SUN Ying-juan, MAI Wen-jie, NIU Li, LI Hong-yan. Potassium storage in bismuth nanoparticles embedded in N-doped porous carbon facilitated by ether-based electrolyte [J]. Chemical Engineering Journal, 2022, 446: 137329.

[22] XIANG Xin-yuan, LIU Dan, ZHU Xin-xin, WANG Ying-ying, QU De-yu, XIE Zhi-zhong, ZHANG Xiong, ZHENG Hua. Boosting interfacial ion transfer in potassium-ion batteries via synergy between nanostructured Bi@NC bulk anode and electrolyte [J]. ACS Applied Materials & Interfaces, 2022, 14(30): 34722−34732.

[23] XUE Pan, WANG Na-na, FANG Zhi-wei, LU Zhen-xiao, XU Xun, WANG Liang, DU Yi, REN Xiao-chun, BAI Zhong-chao, DOU Shi-xue, YU Gui-hua. Rayleigh-instability-induced bismuth nanorod@nitrogen-doped carbon nanotubes as a long cycling and high rate anode for sodium-ion batteries [J]. Nano Letters, 2019, 19(3): 1998−2004.

[24] XIONG Pei-xun, BAI Pan-xing, LI Ang, LI Ben-fang, CHENG Ming-ren, CHEN Yi-ping, HUANG Shu-ping, JIANG Qiang, BU Xian-he, XU Yun-hua. Bismuth nanoparticle@carbon composite anodes for ultralong cycle life and high-rate sodium-ion batteries [J]. Advanced Materials, 2019, 31(48): e1904771.

[25] LI Wen-na, GAO Neng-shuang, LI He-chen, SUN Rui-cong, LIU Qing-quan, HUANG Bin, CHEN Quan-qi. Bi@Bi_2O_3 anchored on porous graphene prepared by solvothermal method as a high-performance anode material for potassium-ion batteries [J]. Journal of Alloys and Compounds, 2023, 939: 168766.

[26] LIU Miao, ZHANG Jun-fei, SUN Zhen, HUANG Lu, XIE Tian, WANG Xian-wen, WANG Dong, WU Ying-peng. Dual mechanism for sodium based energy storage [J]. Small, 2023, 19(15): 2206922.

[27] SU Da-wei, DOU Shi-xue, WANG Guo-xiu. Bismuth: A new anode for the Na-ion battery [J]. Nano Energy, 2015, 12: 88−95.

[28] ZHOU Jing, CHEN Jiang-chun, CHEN Meng-xue, WANG Jun, LIU Xiao-zhi, WEI Bin, WANG Zhong-chang, LI Jun-jie, GU Lin, ZHANG Qing-hua, WANG Hua, GUO Lin. Few-layer bismuthene with anisotropic expansion for high-areal-capacity sodium-ion batteries [J]. Advanced Materials, 2019, 31(12): e1807874.

[29] WANG Liu-bin, WANG Chen-chen, LI Fu-jun, CHENG Fang-yi, CHEN Jun. In situ synthesis of Bi nanoflakes on Ni foam for sodium-ion batteries [J]. Chemical Communications, 2017, 54(1): 38−41.

[30] YIN Hong, LI Qing-wei, CAO Ming-lei, ZHANG Wei, ZHAO Han, LI Chong, HUO Kai-fu, ZHU Ming-qiang. Nanosized-bismuth-embedded 1D carbon nanofibers as high-performance anodes for lithium-ion and sodium-ion batteries [J]. Nano Research, 2017, 10(6): 2156−2167.

[31] SADAN M K, SONG E, YU H, YUN J, KIM T M, AHN J H, CHO K K, AHN H J. Extended cycling performance of micron-sized bismuth anodes for lithium-ion batteries: Self-healing of an alloy-type anode for lithium batteries [J]. Journal of Materials Chemistry A, 2023, 11(28): 15466−15474.

[32] HUANG Yu-zhu, XING Lin, PEI Shuang, ZHOU Wei, HU Yu-jie, DENG Wei-na, CHEN Liang, ZHU Hai, CHEN Han, Co_9S_8/CNTs microspheres as superior-performance cathodes in aqueous ammonium-ion batteries [J]. Transactions of Nonferrous Metals Society of China, 2023, 33(11): 3452−3464.

[33] LI Sheng-yang, ZHANG Qiu-sheng, DENG Hong-li, CHEN Song, SHEN Xiao-hua, YUAN Yi-zhi, CHENG Ying-liang, ZHU Jian, LU Bin-gan. Confined bismuth-organic framework anode for high-energy potassium-ion batteries [J]. Small Methods, 2023, 7(6): e2201554.

[34] ZHOU Jing, DING Yang, WANG Ying-yu, LI Hao-yu, SHANG Jia-yi, CAO Yu, WANG Hua. Bulk bismuth anodes for wide-temperature sodium-ion batteries enabled by electrolyte chemistry modulation [J]. Journal of Colloid and Interface Science, 2024, 657: 502−510.

核壳结构 Bi@介孔碳纳米球作为钠离子电池高倍率和长寿命负极材料

杨 武[1]，杨哲伟[1]，王朝辉[1]，边海楠[1]，潘跃德[1]，李 刚[1]，王开鹰[2]，王接喜[3,4]

1. 太原理工大学 材料科学与工程学院 能源革命创新研究院，太原 030024；
2. Department of Microsystems, University of South-Eastern Norway, Horten 3184, Norway;
3. 中南大学 冶金与环境学院，长沙 410083；
4. 国家先进储能材料工程技术研究中心，长沙 410205

摘 要：为了减缓钠离子电池用铋金属负极在合金化过程中产生的巨大体积膨胀，采用溶胶−凝胶法结合热处理的方法，设计和制备了一种核壳结构 Bi@介孔碳纳米球(Bi@mC)复合材料。结构表征显示，Bi@mC 复合材料的平均直径约为 200 nm，其中 N 掺杂的介孔碳外壳厚度为 20~30 nm。电化学测试以及动力学结果表明，介孔碳外壳不仅能有效缓解由铋金属体积膨胀引起的应力，抑制活性材料在充电/放电过程中由应力造成的粉碎，而且能促进钠离子的快速扩散，从而提高倍率和循环性能。在电流密度为 5 A/g 的条件下，Bi@mC 的比容量高达 279 mA·h/g，循环 3500 次后容量保持率为 97.6%。即使在 20 A/g 的大电流密度条件下，Bi@mC 仍能保持高达 266 mA·h/g 的比容量。此外，以制备的 Bi@mC 材料为负极，磷酸钒钠($Na_3V_2(PO_4)_3$(NVP))为正极，组装成扣式全钠离子电池 Bi@mC//NVP，全电池能够输出 182 W·h/kg 的能量密度。

关键词：钠离子电池；铋；核壳结构；溶胶−凝胶法；动力学分析

(Edited by Wei-ping CHEN)